NANO LETTERS

Letter

pubs.acs.org/NanoLett

$MoSe_2$ and WSe_2 Nanofilms with Vertically Aligned Molecular Layers on Curved and Rough Surfaces

Haotian Wang,[†] Desheng Kong,[‡] Petr Johanes,[‡] Judy J. Cha,[‡] Guangyuan Zheng,[§] Kai Yan,[‡] Nian Liu,[∥] and Yi Cui*[,‡,⊥]

[†]Department of Applied Physics, Stanford University, Stanford, California 94305, United States

[‡]Department of Materials Science and Engineering, Stanford University, Stanford, California 94305, United States

[§]Department of Chemical Engineering, Stanford University, Stanford, California 94305, United States

[∥]Department of Chemistry, Stanford University, Stanford, California 94305, United States

[⊥]Stanford Institute for Materials and Energy Sciences, SLAC National Accelerator Laboratory, 2575 Sand Hill Road, Menlo Park, California 94025, United States

S *Supporting Information*

ABSTRACT: Two-dimensional (2D) layered materials exhibit high anisotropy in materials properties due to the large difference of intra- and interlayer bonding. This presents opportunities to engineer materials whose properties strongly depend on the orientation of the layers relative to the substrate. Here, using a similar growth process reported in our previous study of MoS_2 and $MoSe_2$ films whose layers were oriented vertically on flat substrates, we demonstrate that the vertical layer orientation can be realized on curved and rough surfaces such as nanowires (NWs) and microfibers. Such structures can increase the surface area while maintaining the perpendicular orientation of the layers, which may be useful in enhancing various catalytic activities. We show vertically aligned $MoSe_2$ and WSe_2 nanofilms on Si NWs and carbon fiber paper. We find that $MoSe_2$ and WSe_2 nanofilms on carbon fiber paper are highly efficient electrocatalysts for hydrogen evolution reaction (HER) compared to flat substrates. Both materials exhibit extremely high stability in acidic solution as the HER catalytic activity shows no degradation after 15 000 continuous potential cycles. The HER activity of $MoSe_2$ is further improved by Ni doping.

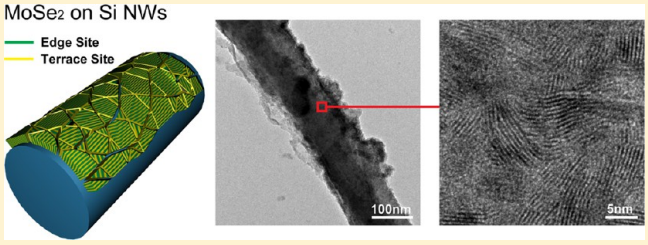

KEYWORDS: *2D material, $MoSe_2$, WSe_2, hydrogen evolution reaction, selenization*

Two-dimensional (2D) materials have intrigued not only fundamental science study but also novel materials engineering due to the unique physical and chemical properties.[1−10] Charge-neutral 2D molecular single layers with strong in-plane chemical bonds stack together via the weak van der Waals interaction to form the bulk material, introducing the high anisotropy and opening up the opportunities to develop various methods of single layer materials synthesis.[1,4,11−16] Besides the single layer flakes, many other interesting morphologies such as thin films, nanoplates, nanoribbons, nanotubes, nanowires, and fullerene-like nanoparticles are made from 2D materials and show broad applications in a variety of areas such as topological insulator,[17−19] chemical and electrochemical intercalation,[8,20,21] electrocatalysis,[22,23] and transistors.[1,4,24] Most 2D materials studied that far including binary dichalcogenides such as MoS_2 and graphene are inclined to be terminated by the basal planes to reduce the exposed edges due to the inherently high surface energy of the edges. However, the edges of some 2D materials are catalytically active for many important electrochemical reactions such as hydrodesulfurization,[25] hydrogen evolution reaction (HER),[22,26] and oxygen reduction reaction.[27] Exposing edges in these cases can therefore boost the catalytic activities.

Recently, we demonstrated thin films of vertically aligned molybdenum disulfide (MoS_2) and molybdenum diselenide ($MoSe_2$) molecular layers on flat substrates.[28] The edges of MoS_2 have been identified to be active sites for HER theoretically and experimentally;[22,26,29,30] thus, the maximally exposed active edge sites showed large exchange current densities in HER.[28] The synthesis of our vertically aligned layers was through Mo reaction with sulfur or selenium vapor. It is proposed that at high temperatures the vapor diffusion along the layers through van der Waals gaps is much faster than that across the layers; thus, the layers naturally orient perpendicularly to flat substrates to expose the edges.[28] However, it is not clear whether such a rapid sulfurization or selenization reaction mechanism can be translated onto rough and curved surfaces. The rough and curved surfaces can increase the surface area and maximize the exposed edge sites.

Received: May 28, 2013
Revised: June 21, 2013

   dx.doi.org/10.1021/nl401944f | *Nano Lett.* XXXX, XXX, XXX−XXX

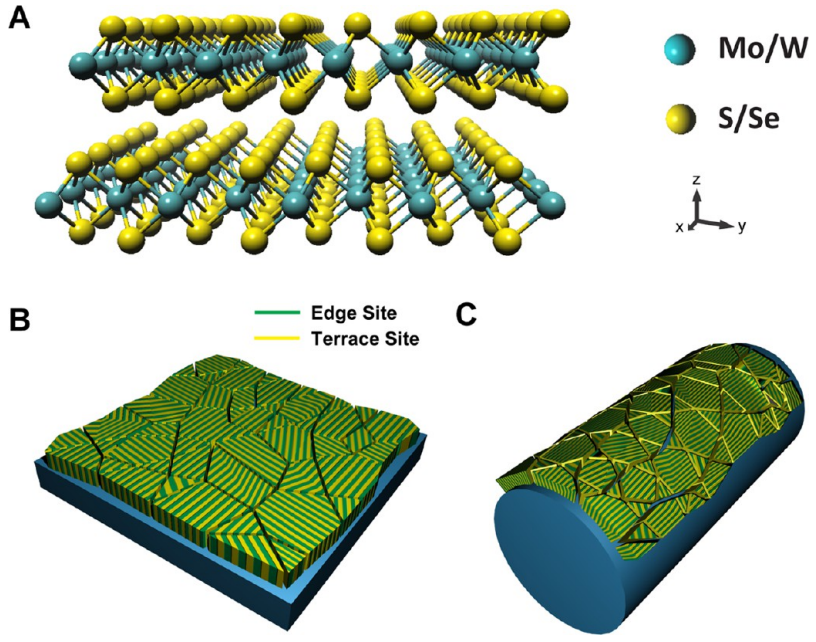

Figure 1. Schematic of $MoSe_2$ and WSe_2 nanostructures. (A) Layered crystal structure of molybdenum (or tungsten) chalcogenide. Each charge-neutral layer consists of three covalently bonded atomic sheets, and the layers stack together along the *c*-axis by van der Waals interaction. (B) Molybdenum (or tungsten) chalcogenide nanofilm with molecular layers vertically standing on a flat substrate. The green color represents the edge sites, and the yellow color represents the terrace sites. (C) Molybdenum (or tungsten) chalcogenide nanofilm with molecular layers perpendicular to a curved surface. The edges are maximally exposed.

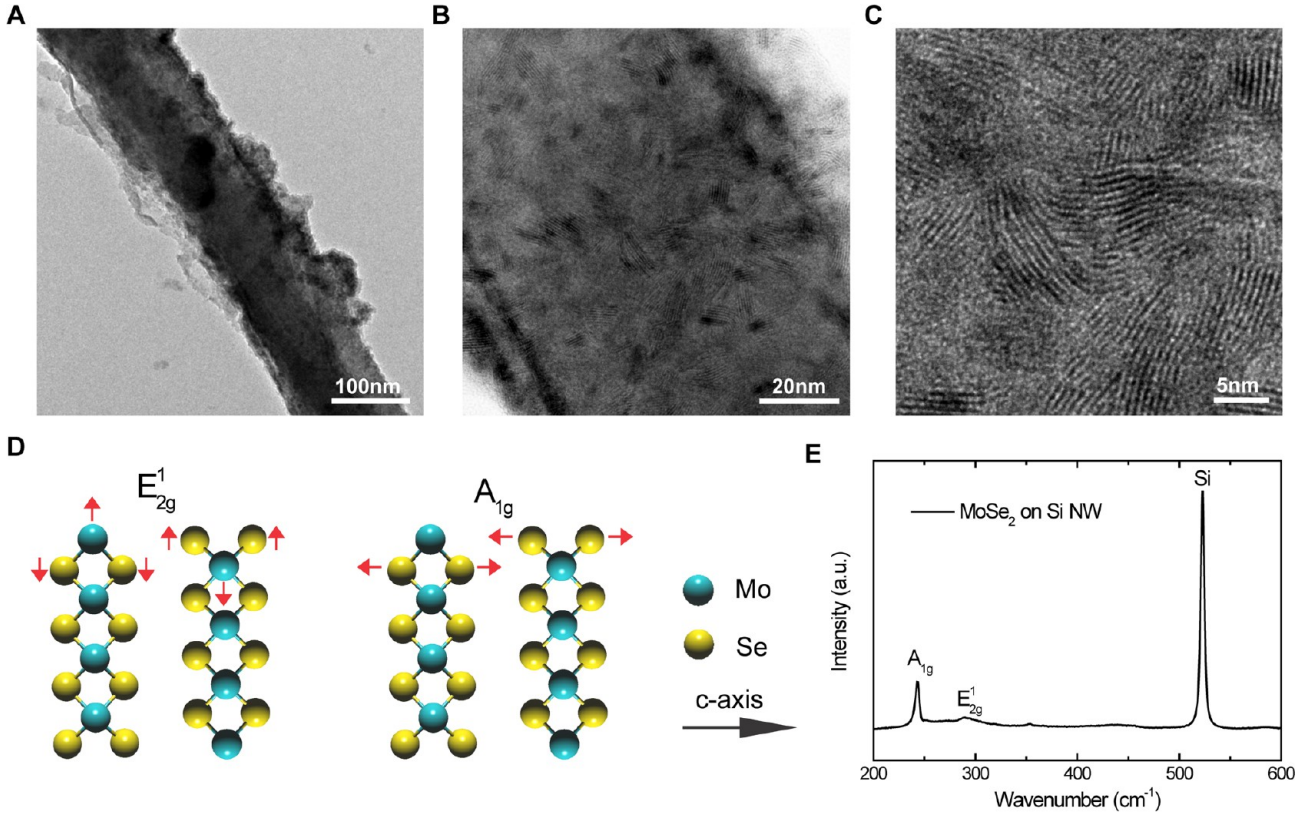

Figure 2. Characterization of $MoSe_2$ nanofilm on a Si NW. (A) TEM image of $MoSe_2$ nanofilm on a Si NW of 100 nm in diameter. (B) TEM image of $MoSe_2$ nanofilm on the curved surface of the Si NW with molecular layers perpendicular to the surface. On the basis of the TEM image, it appears that approximately 80% of the surface is covered with the edges. (C) Zoom-in TEM image of $MoSe_2$ nanofilm on the Si NW. The film is polycrystalline, and the grains are curved and around 10 nm in length and several nanometers in width. (D) The atomic vibration direction of A_{1g} and E^1_{2g} Raman modes of $MoSe_2$. (E) Raman spectrum of $MoSe_2$ nanofilm on Si NWs. The intensity ratio of $MoSe_2$ A_{1g} to E^1_{2g} is around 13:1.

dx.doi.org/10.1021/nl401944f | *Nano Lett.* XXXX, XXX, XXX−XXX

More interestingly, it may also induce strain, expanding or squeezing the molecular layers and thus changing the electronic structures of the films.[31]

Here we demonstrate that $MoSe_2$ and tungsten diselenide (WSe_2) nanofilms with molecular layers perpendicular to rough and curved surfaces can be synthesized by the rapid selenization process, preferentially exposing the active edge sites for HER. We show significant improvement of HER activity of $MoSe_2$ and WSe_2 on carbon fiber paper compared with the flat films. The vertically standing layers create strong bonds to the substrate, resulting in the extremely high electrochemical stability against long-term potential cycling of 15 000 cycles. The HER catalytic activity of the $MoSe_2$ catalysts was further improved by increasing the thickness of the nanofilms or doping with Ni atoms. WSe_2, introduced here, is a novel HER catalyst rarely explored previously.

$MoSe_2$ and WSe_2 share similar crystal structures with MoS_2 as shown in Figure 1A. The atoms covalently bond with each other within single layers, which stack together by van der Waals interaction. Since the surface energy of the edge sites is much larger than that of the terrace sites, for example, in the case of MoS_2 the edge site surface energy is at least 2 orders of magnitude larger than the terrace site surface energy,[32] it is energetically nonfavorable to expose the edge sites on the surface.[22,25,26,33] A kinetically controlled rapid sulfurization or selenization process from our previous work overcomes the barrier, and we synthesized MoS_2 and $MoSe_2$ flat films with molecular layers perpendicular to the substrate, as shown in Figure 1B.[28] The morphology is ideal for HER on a 2D surface by providing high density of edge sites, which have been proven to be the active center of MoS_2 for HER.[22,23,26,28,29,33−40] To further increase the active edge sites per geometric area, the 2D flat substrate might be replaced with high surface area substrates with 2D nanostructures or even 3D porous structures. As illustrated in Figure 1C, making the molecular layers stand on rough and curved surfaces and maximally exposing the edge sites to boost the HER activity is of our interest.

$MoSe_2$ and WSe_2 nanofilms were synthesized on Si nanowires (NWs) with diameters ranging from 100 to 200 nm (Supporting Information Figure S1). The Si NWs were grown by vapor−liquid−solid (VLS) method using gold as catalyst (see Methods).[41] The 5 nm Mo or W films were deposited onto Si NWs by DC magnetron sputtering, followed by a rapid selenization process at 600 °C in a horizontal tube furnace where elementary selenium shots were used as the precursors (see Methods).[28] Because of the directional deposition, only half of the NW surface is covered with the metals. Figure 2A shows the transmission electron microscopy (TEM) image of a $MoSe_2$ nanofilm on a Si NW of ~100 nm in diameter. The dark contrast represents the $MoSe_2$ nanofilm. Figure 2B shows that the curved surface of Si NW is covered by $MoSe_2$ stripelike grains, with molecular layers perpendicular to the NW surface to expose the edges. The edges are distinct along the central axis of the NW because the electron beam is parallel to the vertically standing layers. Away from the central part of the NW, the layers are tilted away from the electron beam; thus, fewer edges are observed. On the basis of TEM images, it appears that approximately 80% of the surface is covered with vertically aligned layers. At the sidewalls of the NW $MoSe_2$ layers shoot out from the surface, again confirming the layers vertically stand along the curved surface.

A zoom-in TEM image is shown in Figure 2C. The grains are around 10 nm long and several nanometers wide, growing in arbitrary directions but with *c*-axis parallel to the surface of the NW. This particular configuration results in a specific intensity ratio of A_{1g} (243 cm^{-1}) to E^1_{2g} (289 cm^{-1}) Raman modes illustrated in Figure 2D,E.[42,43] The Raman peak corresponding to the out-of plane Mo−Se phonon mode (A_{1g}) is preferentially excited for the edge-terminated film, which results in the much higher A_{1g} peak intensity than the E^1_{2g} peak intensity, as shown in Figure 2E (the intensity ratio of A_{1g} to E^1_{2g} is around 13:1).[28,32,44] The presence of Si NWs is confirmed by the strong Raman peak at 523 cm^{-1}.[45] The WSe_2 nanofilm on Si NWs shows similar results to the $MoSe_2$ case, with a part of the curved surface covered by vertically standing layers (Supporting Information Figure S2).

The demonstration of $MoSe_2$ and WSe_2 on Si NWs with molecular layers perpendicular to the surface opens up the opportunity to maximally expose the HER active edge sites on high surface area substrates with curvature and roughness. Accordingly, the HER catalytic activity of $MoSe_2$ and WSe_2 is expected to be largely improved. Carbon fiber paper is used as the substrate which consists of conductive carbon fibers with an average diameter of 10 μm as illustrated in the scanning electron microscopy (SEM) image in Figure 3A. In Figure 3B,

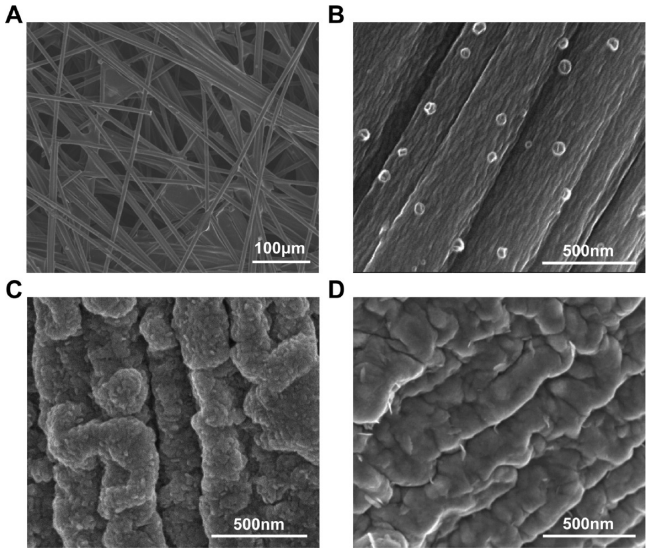

Figure 3. SEM images of bare carbon fiber paper substrates and subsequent $MoSe_2$ and WSe_2 nanofilms on the substrates. (A) SEM image of carbon fiber paper in a large scale. The carbon fibers are hundreds of micrometers in length and around 10 μm in diameter. The junctions are fused together to ensure the conductance of the substrate. (B) SEM image of the rough and curved surface of carbon fiber. There are trenches along the *z*-axis separating the surface area into several regions, with randomly distributed particles on it. (C, D) SEM images of $MoSe_2$ and WSe_2 nanofilms on carbon fiber paper. The films are rough, and the trenches are still visible.

the whole surface of the carbon fiber is separated into rough and curved regions by several trenches, with small particle-like protrusions randomly distributed on the surface. 25 nm thick Mo or W was directionally deposited onto the substrate by dc magnetron sputtering, which was then converted into a corresponding diselenide film by rapid selenization process (see Methods). Figures 3C and 3D show the SEM images of the $MoSe_2$ and WSe_2 nanofilms on the carbon fibers,

dx.doi.org/10.1021/nl401944f | Nano Lett. XXXX, XXX, XXX−XXX

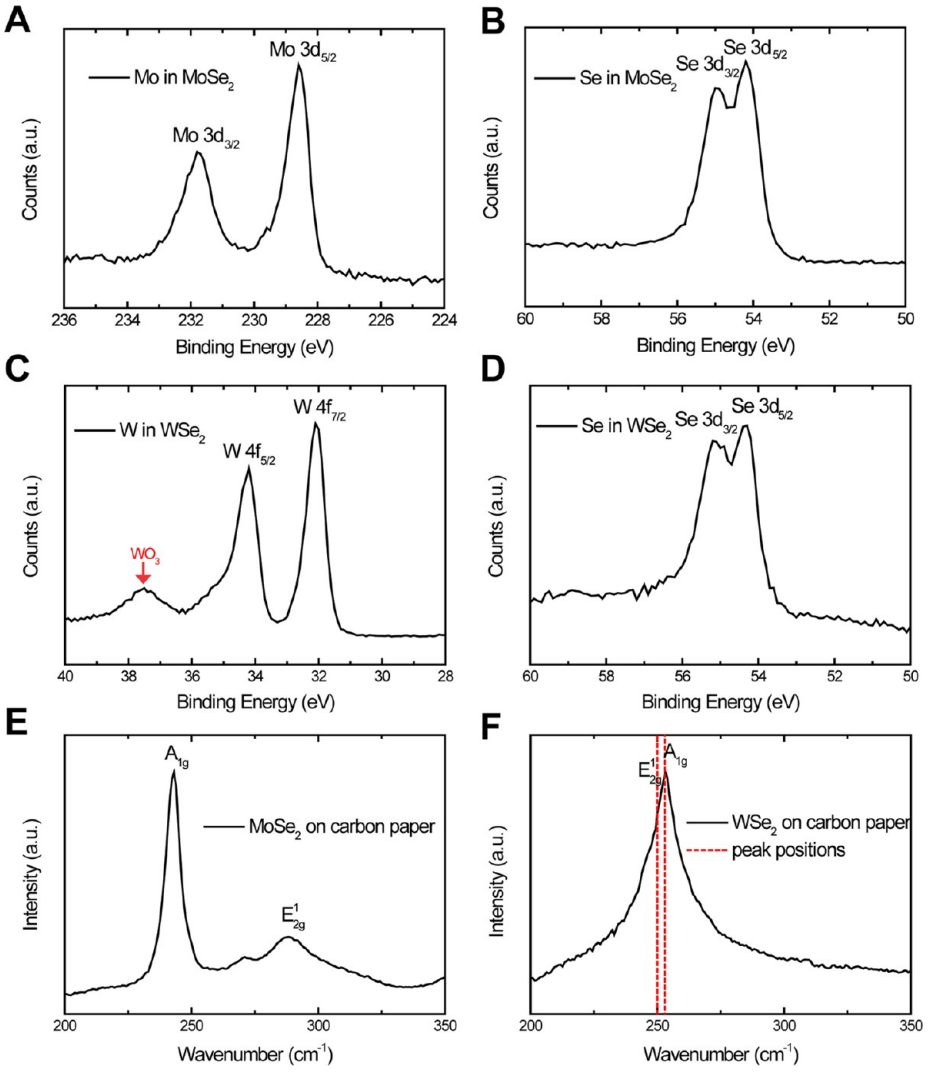

Figure 4. XPS and Raman spectra of $MoSe_2$ and WSe_2 nanofilms on carbon fiber paper. (A, B) High-resolution XPS spectra of Mo 3d and Se 3d regions of $MoSe_2$ nanofilm. (C, D) High-resolution XPS spectra of W 4f and Se 3d regions of WSe_2 nanofilm. The WO_3 peak is indicated by the red arrow. (E) A_{1g} and E^1_{2g} Raman modes of $MoSe_2$ nanofilm. The intensity ratio of the two modes resembles that of the $MoSe_2$ nanofilm on Si NWs. (E) A_{1g} and E^1_{2g} Raman modes of WSe_2 nanofilm. The red dashed lines represent the position of two modes from a previous study.[50]

respectively. The nanofilms turn out to be rough but form continuous coatings on the fibers. The trenches observed in both nanofilms may be related to the surface topographic features of the carbon fibers in Figure 3B. Different from the smooth films synthesized on the mirror polished glassy carbon,[28] the nanofilms on the carbon fiber papers exhibit cluster structures inherited from the surface structures and local curvatures of the fibers.

The $MoSe_2$ and WSe_2 nanofilms were investigated by X-ray photoelectron spectroscopy (XPS) and Raman spectroscopy shown in Figure 4. The binding energies of Mo $3d_{5/2}$ and Mo $3d_{3/2}$ are 228.6 and 231.8 eV in Figure 4A, respectively, revealing the +4 oxidation chemical state of Mo.[33−36,38,46−48] Se $3d_{5/2}$ and Se $3d_{3/2}$ located at 54.2 and 55.0 eV exhibit around the same peak positions for both $MoSe_2$ and WSe_2, as shown in Figures 4B and 4D, indicating the same oxidation state of −2 for Se in both materials.[46−49] The peaks of W $4f_{7/2}$ (32.1 eV) and W $4f_{5/2}$ (34.2 eV) agree well with a previous study of WSe_2 thin films.[49] The small peak at around 37.5 eV in Figure 4C is assigned as W $4f_{5/2}$ from WO_3 due to the oxidation during the sample preparation and transfer, and the W $4f_{7/2}$ from WO_3 at 35.7 eV is buried by the strong peak of W $4f_{5/2}$ from WSe_2.

Raman spectra provide information on the orientation of $MoSe_2$ and WSe_2 molecular layers on the rough and curved surfaces of carbon fiber paper. The Raman modes A_{1g} and E^1_{2g} of $MoSe_2$ are indentified at 243 and 289 cm^{-1} in Figure 4E, respectively, sharing similar intensity ratio (A_{1g}:E^1_{2g} = 13:1) with that of $MoSe_2$ nanofilm on Si NWs. The intensity ratio indicates that the $MoSe_2$ molecular layers are vertically aligned on the carbon fibers, resulting in an edge-terminated nanofilm as designed in Figure 1C which is favorable to improve $MoSe_2$ HER catalytic activity. In addition, this special texture of the nanofilm not only makes full use of the high intralayer conductivity to reduce the impedance of the nanofilm (Supporting Information Figure S3) but also forms strong bonding with the substrate which may improve the stability of the nanofilm. The A_{1g} and E^1_{2g} modes of WSe_2 are closely located at 253 and 250 cm^{-1}, respectively.[50] Accordingly, the two Raman mode peaks cannot be distinguished and only one broad peak is observed in Figure 4F. However, the A_{1g} peak can still be identified as the stronger peak.[50] Furthermore, the peak

dx.doi.org/10.1021/nl401944f | Nano Lett. XXXX, XXX, XXX−XXX

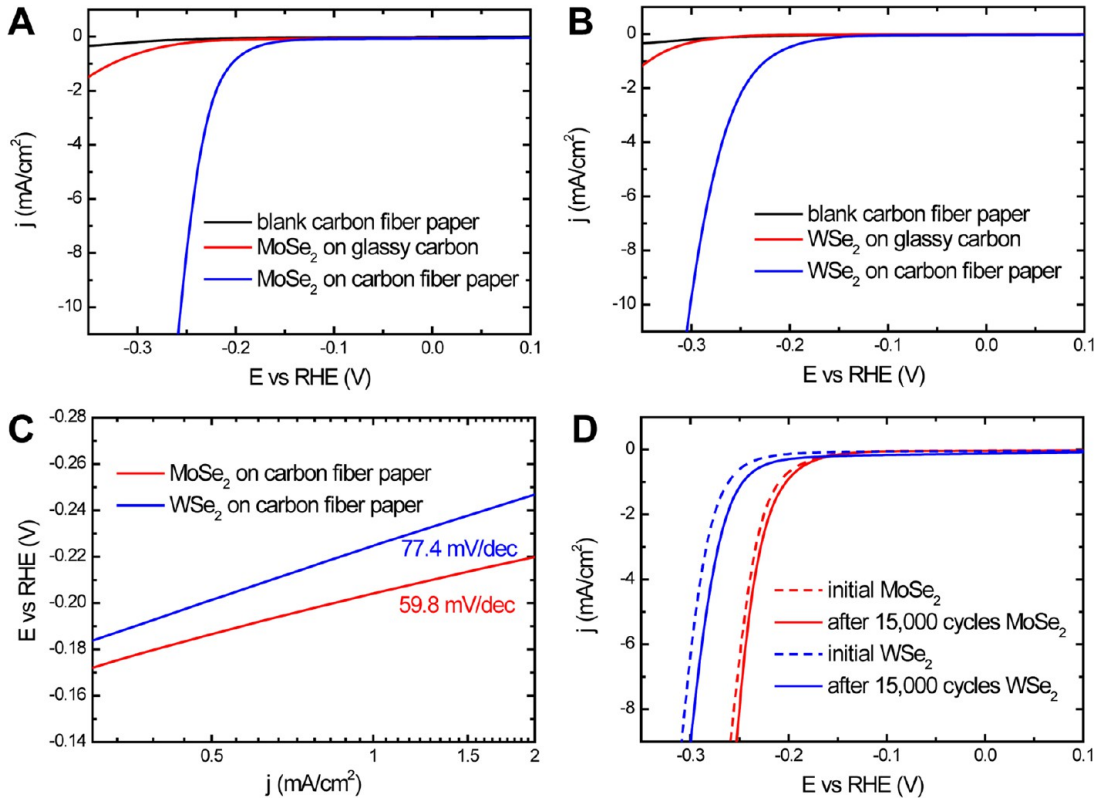

Figure 5. HER catalytic activities of $MoSe_2$ and WSe_2 nanofilms on carbon fiber paper. (A, B) Cathodic polarization curves of $MoSe_2$ and WSe_2 nanofilms on carbon fiber paper compared with those on mirror polished glassy carbon as well as a blank carbon fiber paper substrate. (C) Tafel plots of $MoSe_2$ and WSe_2 nanofilms on carbon fiber paper. (D) Electrochemical stability test of $MoSe_2$ and WSe_2 in the cathodic potentials windows.

shares the same position and shape with that of WSe_2 nanofilm on Si NWs (Figure S2); therefore, it is expected that the edges of WSe_2 are also preferentially exposed on the surface of carbon fiber paper.

The HER catalytic activity of $MoSe_2$ and WSe_2 nanofilms on carbon fiber paper substrates are studied in 0.5 M H_2SO_4 solution with a typical three-electrode electrochemical cell setup. Electrochemical impedance spectroscopy (EIS) reveals negligible ohmic resistance of the nanofilms (Figure S3). Since the electrochemical cell contains series resistances in the wiring, solution, and substrate, all of the data have been *iR*-corrected by subtracting the ohmic resistance loss from the overpotential. The cathodic polarization curves of $MoSe_2$ and WSe_2 nanofilms on carbon fiber paper at a slow scan rate of 2 mV/s are shown in Figures 5A and 5B. In the $MoSe_2$ electrode case, the reduction current density reaches 10 mA/cm^2 at an overpotential around −250 mV, with much higher activity than the vertically aligned $MoSe_2$ film grown on flat, mirror polished glassy carbon in our previous study.[28] Although WSe_2 has lower activity than $MoSe_2$ with 50 mV larger overpotential to drive cathodic current density of 10 mA/cm^2, it is still interesting because WSe_2 has never been reported to be a good electrocatalyst for HER. Here WSe_2 exhibits much higher HER activity than that of WS_2 reported before.[34,37,51] Notice that WSe_2 can be used as photocathode; our finding suggests the possibility to use WSe_2 as both light absorber and HER catalyst in photoelectrochemical cells.[52−54]

Tafel plots in Figure 5C are used to determine two important parameters describing HER activity of catalysts: Tafel slope and exchange current density. The linear part of the $MoSe_2$ Tafel plot under small overpotential is fitted to give a Tafel slope of 59.8 mV/dec, which is much smaller than the 120 mV/dec from $MoSe_2$ on mirror polished glassy carbon.[28] The exchange current density is determined to be 3.8×10^{-4} mA/cm^2 by fitting the linear portion of the Tafel plot at low cathodic current to the Tafel equation.[22,28] Tafel slope is associated with the elementary steps in HER. The first step of HER is a discharge step (Volmer reaction) in which protons are adsorbed to active sites on the surface of the catalysts and combined with electrons to form adsorbed hydrogen atoms.[26,40,55,56] It is followed by a combination step (Tafel reaction) or a desorption step (Heyrovsky reaction). In the previous work the observed 120 mV/dec Tafel slope of $MoSe_2$ on flat glassy carbon substrate indicates that the rate-determining step was the discharge step, with a very small surface coverage of adsorbed hydrogen.[28,56,57] In this work, it seems that the free energy barrier of the discharge step is reduced to be comparable with that of the following desorption or combination step, resulting in the slope of 59.8 mV/dec.[36,39] The surface curvature and roughness of the carbon fiber paper substrate are likely to be responsible for the improved Tafel slope. The roughness and surface curvature may be able to expand or squeeze the vertically standing molecular layers and thus change the electronic properties of the nanofilms, which may tune the reaction barriers effectively.[28,33] WSe_2 nanofilm on carbon fiber paper with a Tafel slope of 77.4 mV/dec also exhibits the facile HER kinetic process, which is a promising candidate in self-catalyzing HER in photoelectrochemical cells.[52−54]

The structure of $MoSe_2$ and WSe_2 nanofilms with molecular layers perpendicular to the substrates is beneficial to the stability of the catalysts due to the strong bonds between the

dx.doi.org/10.1021/nl401944f | *Nano Lett.* XXXX, XXX, XXX−XXX

layers and the substrates. The extremely high stability of both $MoSe_2$ and WSe_2 nanofilms is shown in Figure 5D. The as-grown catalysts were cycled by taking continuous cyclic voltammograms (CV) between −0.28 and 0.1 V for $MoSe_2$ and −0.32 and 0.1 V for WSe_2 vs RHE (before *iR* correction), respectively, over 15 000 cycles at a rate of 50 mV/s. The lower potential limits were set to reach a high cathodic current density of 10 mA/cm^2. We gently cleaned the surface of the $MoSe_2$ and WSe_2 catalysts and acquired polarization curves every 1000 CV cycles. The activities of both catalysts after 15 000 cycles are slightly improved, likely due to the removal of the surface contaminates. The result confirms the extremely high stability of $MoSe_2$ and WSe_2 catalysts on carbon fiber paper. The SEM images of $MoSe_2$ and WSe_2 nanofilms on carbon fiber paper after the cycling confirm that the nanofilms are still tightly adhered to the carbon fibers, without any visible degradation (Figure S4).

The HER catalytic activity of the catalysts can be further improved by increasing the thickness of the nanofilms. This is demonstrated by $MoSe_2$ shown in Figure 6. We deposited 50 nm of Mo onto the substrate, using the same procedure to convert the Mo film into $MoSe_2$. The thickness of the $MoSe_2$ nanofilm was around 200 nm. (Previously, we deposited 25 nm of Mo onto the carbon fiber paper, which resulted in ∼100 nm thick $MoSe_2$ nanofilm.) The measured Tafel slope of the thicker $MoSe_2$ nanofilm is maintained to be 63.9 mV/dec, but the exchange current density is increased to 1.3 × 10^{-3} mA/cm^2. Comparing with the thinner $MoSe_2$ nanofilm, the thicker one may cover more surface area of the carbon fiber paper, and the surface may also be rougher. However, the 200 nm thick $MoSe_2$ nanofilm does not share the comparable stability with the thinner one. The activity of the 200 nm $MoSe_2$ nanofilm substantially decays after 1000 potential cycles (Figure S5). The stability issue is associated with the poor mechanical adhesion of the active catalyst with the carbon fibers as revealed by the SEM images after cycling (Figure S6). Unlike the thinner $MoSe_2$ film, the thicker film does not bond to the substrate strongly enough and a large part of the film was easily peeled off during the operation. We suspect that the induced strain is much larger for a thicker nanofilm which weakens the bonding to the substrate. It suggests the thickness of the nanofilm should be optimized to balance the catalytic activity and the stability for long-term operation.

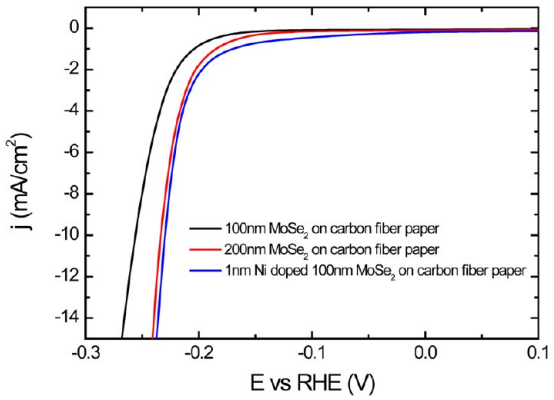

Figure 6. Further improvement of HER catalytic activity of $MoSe_2$ nanofilm on carbon fiber paper. The black line represents the polarization curve of the pristine $MoSe_2$ catalyst, the red one stands for the double-thickness $MoSe_2$ nanofilm, and the blue one is the Ni-doped $MoSe_2$ nanofilm.

It is known the incorporation of transition metals like Co, Ni, and Fe into WS_2 and MoS_2 enhances their catalytic activity for HER.[34,39] In the MoS_2 case, the hydrogen binding energy at the Mo-edge is smaller than that at the S-edge; accordingly, only the Mo-edge is catalytically active for HER.[26,34,39] The Co-promoted S-edge significantly reduce the hydrogen binding free energy, making the S-edge active for HER.[34,39] Inspired by these theoretical calculations and experimental results, we doped a small amount of Ni atoms into $MoSe_2$ and explored its influence on the catalytic activity. An additional 5 Å thick Ni was thermally evaporated onto the 5 nm Mo film on Si NWs, followed by the rapid selenization process. The TEM image of the Ni-doped $MoSe_2$ nanofilm on Si NWs is shown in Figure S8, confirming that the vertically aligned $MoSe_2$ molecular layers were not affected by Ni doping. No Ni−Se clusters are observed in the TEM image, indicating that the Ni atoms are homogeneously incorporated into the $MoSe_2$ matrix. To obtain the HER catalytic activity, Ni-doped $MoSe_2$ nanofilms were synthesized on carbon fiber paper with 1 nm thick Ni thermally evaporated onto 25 nm thick Mo film. Ni doping enhances the activity by increasing the exchange current density to 2.8 × 10^{-3} mA/cm^2 without affecting the Tafel slope (62.1 mV/dec). Accordingly, the Ni-doped catalyst achieves a cathodic current density of 10 mA/cm^2 with 30 mV lower overpotential than the pristine $MoSe_2$ catalyst.

In conclusion, we used the rapid selenization process to synthesize $MoSe_2$ and WSe_2 on Si NWs and carbon microfibers with molecular layers perpendicular to the curved and rough surfaces. With the unique layer orientation that maximally exposes the edge sites of the material, we produced highly active catalysts for HER. The catalytic activity of $MoSe_2$ on the curved and rough surfaces is demonstrated to be much higher than that of $MoSe_2$ on the flat substrate. WSe_2 is introduced here as a novel active HER catalyst which may function as both light absorber and HER catalyst in photoelectrochemical cells. Both materials exhibit extremely high stability thanks to the strong bonding between the layers and the substrate. These edge-terminated layered catalysts can be readily applied in diverse water electrolysis devices as low-cost, high-performance, and stable HER catalysts.

Methods. *Synthesis and Preparation.* 30 nm thick Au film was thermally evaporated onto the Si substrate to be the catalyst for Si NWs growth by the VLS method. Single-crystalline Si NWs were grown inside a tube furnace at 485 °C for 20 min, with silane (SiH_4, 2% in Ar) flowed in at 80 sccm and hydrogen (H_2, 99.999%) at 20 sccm with a total chamber pressure of 30 Torr. Edge-terminated $MoSe_2$ and WSe_2 nanofilms on Si NWs and carbon fiber paper were grown inside a single-zone, 12 in. horizontal tube furnace (Lindberg/Blue M) equipped with a 1 in. diameter quartz tube. The substrates coated with Mo or W thin films were placed at the hot center of the tube furnace. Selenium shots (99.99%, from Alfa Aesar) were placed on the upstream side of the furnace at carefully adjusted locations to set the temperature. Ar gas was used as the precursor carrier, and the pressure and flow rate were kept at 1000 mTorr and 100 sccm, respectively, during the growth. The heating center of the furnace was quickly raised to reaction temperature of 600 °C in 15 min, and the selenium precursor was kept at around 300 °C. The furnace was held at reaction temperature for 15 min, followed by natural cool-down.

dx.doi.org/10.1021/nl401944f | *Nano Lett.* XXXX, XXX, XXX−XXX

Characterizations. Characterizations were carried out using transmission electron spectroscopy (TEM, FEI Tecnai G2 F20 X-Twin microscope at 200 keV), Raman spectroscopy (531 nm excitation laser, WITEC Raman spectrometer), X-ray photoelectron spectroscopy (XPS, SSI SProbe XPS spectrometer with Al Kα source), and scanning electron microscopy (SEM, FEI Nova NanoSEM 450).

Electrochemical Studies. $MoSe_2$ and WSe_2 nanofilms were grown on carbon fiber paper (from Fuel Cell Store) to measure HER activities. Electrochemically inert Kapton tape was used to define the 1 cm^2 electrode area. The measurements were performed in 0.5 M H_2SO_4 solution (deaerated by N_2) using a three-electrode electrochemical cell setup, with a saturated calomel electrode (E(RHE) = E(SCE) + 0.279 V after calibration) as the reference electrode and a graphite rod (99.999%, from Sigma-Aldrich) as the counter electrode.

■ ASSOCIATED CONTENT

Ⓢ Supporting Information

Additional details on sample chracterizations, electrochemical measurements, and analyses. This material is available free of charge via the Internet at http://pubs.acs.org.

■ AUTHOR INFORMATION

Corresponding Author

*E-mail: yicui@stanford.edu (Y.C.).

Notes

The authors declare no competing financial interest.

■ ACKNOWLEDGMENTS

We acknowledge support by the Department of Energy, Office of Basic Energy Sciences, Materials Sciences and Engineering Division, under Contract DE-AC02-76-SFO0515. Author contributions are as follows: H.W., D.K., and Y.C. conceived the experiments. H.W., P.J., and N.L. synthesized and prepared the materials. H.W., D.K., J.J.C., and G.Z. performed characterizations. H.W., D.K., and P.J. carried out electrochemical measurements and analyses. All authors contributed to scientific planning and discussions.

■ REFERENCES

(1) Novoselov, K. S.; Geim, A. K.; Morozov, S. V.; Jiang, D.; Zhang, Y.; Dubonos, S. V.; Grigorieva, I. V.; Firsov, A. A. *Science* **2004**, *306* (5696), 666−669.

(2) Novoselov, K. S.; Jiang, D.; Schedin, F.; Booth, T. J.; Khotkevich, V. V.; Morozov, S. V.; Geim, A. K. *Proc. Natl. Acad. Sci. U. S. A.* **2005**, *102* (30), 10451−10453.

(3) Geim, A. K.; Novoselov, K. S. *Nat. Mater.* **2007**, *6* (3), 183−191.

(4) Radisavljevic, B.; Radenovic, A.; Brivio, J.; Giacometti, V.; Kis, A. *Nat. Nanotechnol.* **2011**, *6* (3), 147−150.

(5) Splendiani, A.; Sun, L.; Zhang, Y.; Li, T.; Kim, J.; Chim, C.-Y.; Galli, G.; Wang, F. *Nano Lett.* **2010**, *10* (4), 1271−1275.

(6) Hasan, M. Z.; Kane, C. L. *Rev. Mod. Phys.* **2010**, *82* (4), 3045−3067.

(7) Zhang, H.; Liu, C.-X.; Qi, X.-L.; Dai, X.; Fang, Z.; Zhang, S.-C. *Nat. Phys.* **2009**, *5* (6), 438−442.

(8) Mizushima, K.; Jones, P. C.; Wiseman, P. J.; Goodenough, J. B. *Mater. Res. Bull.* **1980**, *15* (6), 783−789.

(9) Tenne, R.; Margulis, L.; Genut, M.; Hodes, G. *Nature* **1992**, *360* (6403), 444−446.

(10) Liu, Y.-H.; Porter, S. H.; Goldberger, J. E. *J. Am. Chem. Soc.* **2012**, *134* (11), 5044−5047.

(11) Hernandez, Y.; Nicolosi, V.; Lotya, M.; Blighe, F. M.; Sun, Z.; De, S.; McGovern, I. T.; Holland, B.; Byrne, M.; Gun'Ko, Y. K.; Boland, J. J.; Niraj, P.; Duesberg, G.; Krishnamurthy, S.; Goodhue, R.; Hutchison, J.; Scardaci, V.; Ferrari, A. C.; Coleman, J. N. *Nat. Nanotechnol.* **2008**, *3* (9), 563−568.

(12) Ramakrishna Matte, H. S. S.; Gomathi, A.; Manna, A. K.; Late, D. J.; Datta, R.; Pati, S. K.; Rao, C. N. R. *Angew. Chem.* **2010**, *122* (24), 4153−4156.

(13) Reina, A.; Jia, X.; Ho, J.; Nezich, D.; Son, H.; Bulovic, V.; Dresselhaus, M. S.; Kong, J. *Nano Lett.* **2008**, *9* (1), 30−35.

(14) Balandin, A. A.; Ghosh, S.; Bao, W.; Calizo, I.; Teweldebrhan, D.; Miao, F.; Lau, C. N. *Nano Lett.* **2008**, *8* (3), 902−907.

(15) Kim, F.; Cote, L. J.; Huang, J. *Adv. Mater.* **2010**, *22* (17), 1954−1958.

(16) Eda, G.; Yamaguchi, H.; Voiry, D.; Fujita, T.; Chen, M.; Chhowalla, M. *Nano Lett.* **2011**, *11* (12), 5111−5116.

(17) Chen, Y. L.; Analytis, J. G.; Chu, J.-H.; Liu, Z. K.; Mo, S.-K.; Qi, X. L.; Zhang, H. J.; Lu, D. H.; Dai, X.; Fang, Z.; Zhang, S. C.; Fisher, I. R.; Hussain, Z.; Shen, Z.-X. *Science* **2009**, *325* (5937), 178−181.

(18) Peng, H.; Lai, K.; Kong, D.; Meister, S.; Chen, Y.; Qi, X.-L.; Zhang, S.-C.; Shen, Z.-X.; Cui, Y. *Nat. Mater.* **2010**, *9* (3), 225−229.

(19) Kong, D.; Randel, J. C.; Peng, H.; Cha, J. J.; Meister, S.; Lai, K.; Chen, Y.; Shen, Z.-X.; Manoharan, H. C.; Cui, Y. *Nano Lett.* **2009**, *10* (1), 329−333.

(20) Shu, Z. X.; McMillan, R. S.; Murray, J. J. *J. Electrochem. Soc.* **1993**, *140* (4), 922−927.

(21) Koski, K. J.; Cha, J. J.; Reed, B. W.; Wessells, C. D.; Kong, D.; Cui, Y. *J. Am. Chem. Soc.* **2012**, *134* (18), 7584−7587.

(22) Jaramillo, T. F.; Jorgensen, K. P.; Bonde, J.; Nielsen, J. H.; Horch, S.; Chorkendorff, I. *Science* **2007**, *317* (5834), 100−102.

(23) Chen, Z.; Cummins, D.; Reinecke, B. N.; Clark, E.; Sunkara, M. K.; Jaramillo, T. F. *Nano Lett.* **2011**, *11* (10), 4168−4175.

(24) Li, X.; Wang, X.; Zhang, L.; Lee, S.; Dai, H. *Science* **2008**, *319* (5867), 1229−1232.

(25) Prins, R.; De Beer, V. H. J.; Somorjai, G. A. *Catal. Rev.* **1989**, *31* (1−2), 1−41.

(26) Hinnemann, B.; Moses, P. G.; Bonde, J.; Jorgensen, K. P.; Nielsen, J. H.; Horch, S.; Chorkendorff, I.; Norskov, J. K. *J. Am. Chem. Soc.* **2005**, *127* (15), 5308−5309.

(27) Ahmed, S. M.; Gerischer, H. *Electrochim. Acta* **1979**, *24* (6), 705−711.

(28) Kong, D.; Wang, H.; Cha, J. J.; Pasta, M.; Koski, K. J.; Yao, J.; Cui, Y. *Nano Lett.* **2013**, *13* (3), 1341−1347.

(29) Jaramillo, T. F.; Bonde, J.; Zhang, J.; Ooi, B.-L.; Andersson, K.; Ulstrup, J.; Chorkendorff, I. *J. Phys. Chem. C* **2008**, *112* (45), 17492−17498.

(30) Karunadasa, H. I.; Montalvo, E.; Sun, Y.; Majda, M.; Long, J. R.; Chang, C. J. *Science* **2012**, *335* (6069), 698−702.

(31) Allan, D. R.; Kelsey, A. A.; Clark, S. J.; Angel, R. J.; Ackland, G. J. *Phys. Rev. B* **1998**, *57* (9), 5106−5110.

(32) Verble, J. L.; Wietling, T. J.; Reed, P. R. *Solid State Commun.* **1972**, *11* (8), 941−944.

(33) Kibsgaard, J.; Chen, Z.; Reinecke, B. N.; Jaramillo, T. F. *Nat. Mater.* **2012**, *11* (11), 963−969.

(34) Bonde, J.; Moses, P. G.; Jaramillo, T. F.; Norskov, J. K.; Chorkendorff, I. *Faraday Discuss.* **2008**, *140* (0), 219−231.

(35) Benck, J. D.; Chen, Z.; Kuritzky, L. Y.; Forman, A. J.; Jaramillo, T. F. *ACS Catal.* **2012**, *2* (9), 1916−1923.

(36) Merki, D.; Fierro, S.; Vrubel, H.; Hu, X. *Chem. Sci.* **2011**, *2* (7), 1262−1267.

(37) Merki, D.; Hu, X. *Energy Environ. Sci.* **2011**, *4* (10), 3878−3888.

(38) Vrubel, H.; Merki, D.; Hu, X. *Energy Environ. Sci.* **2012**, *5* (3), 6136−6144.

(39) Merki, D.; Vrubel, H.; Rovelli, L.; Fierro, S.; Hu, X. *Chem. Sci.* **2012**, *3* (8), 2515−2525.

(40) Li, Y.; Wang, H.; Xie, L.; Liang, Y.; Hong, G.; Dai, H. *J. Am. Chem. Soc.* **2011**, *133* (19), 7296−7299.

(41) Chan, C. K.; Peng, H.; Liu, G.; McIlwrath, K.; Zhang, X. F.; Huggins, R. A.; Cui, Y. *Nat Nanotechnol.* **2008**, *3* (1), 31−35.

(42) Sekine, T.; Izumi, M.; Nakashizu, T.; Uchinokura, K.; Matsuura, E. *J. Phys. Soc. Jpn.* **1980**, *49* (3), 1069.

(43) Wieting, T. J.; Verble, J. L. *Phys. Rev. B* **1971**, *3* (12), 4286–4292.
(44) Verble, J. L.; Wieting, T. J. *Phys. Rev. Lett.* **1970**, *25* (6), 362–365.
(45) Richter, H.; Wang, Z. P.; Ley, L. *Solid State Commun.* **1981**, *39* (5), 625–629.
(46) Abdallah, W.; Nelson, A. E. *J. Mater. Sci.* **2005**, *40* (9–10), 2679–2681.
(47) Pouzet, J.; Bernede, J. C. *Rev. Phys. Appl.* **1990**, *25* (8), 807–815.
(48) Ohuchi, F. S.; Parkinson, B. A.; Ueno, K.; Koma, A. *J. Appl. Phys.* **1990**, *68* (5), 2168–2175.
(49) Boscher, N. D.; Carmalt, C. J.; Parkin, I. P. *J. Mater. Chem.* **2006**, *16* (1), 122–127.
(50) Mead, D. G.; Irwin, J. C. *Can. J. Phys.* **1977**, *55* (5), 379–382.
(51) Sobczynski, A.; Yildiz, A.; Bard, A. J.; Campion, A.; Fox, M. A.; Mallouk, T.; Webber, S. E.; White, J. M. *J. Phys. Chem.* **1988**, *92* (8), 2311–2315.
(52) McKone, J. R.; Pieterick, A. P.; Gray, H. B.; Lewis, N. S. *J. Am. Chem. Soc.* **2013**, *135* (1), 223–231.
(53) Boettcher, S. W.; Warren, E. L.; Putnam, M. C.; Santori, E. A.; Turner-Evans, D.; Kelzenberg, M. D.; Walter, M. G.; McKone, J. R.; Brunschwig, B. S.; Atwater, H. A.; Lewis, N. S. *J. Am. Chem. Soc.* **2011**, *133* (5), 1216–1219.
(54) Liu, C.; Tang, J.; Chen, H. M.; Liu, B.; Yang, P. *Nano Lett.* **2013**, in press.
(55) Conway, B. E.; Tilak, B. V. *Electrochim. Acta* **2002**, *47* (22–23), 3571–3594.
(56) Thomas, J. G. N. *Trans. Faraday Soc.* **1961**, *57*, 1603–1611.
(57) Pentland, N.; Bockris, J. O. M.; Sheldon, E. *J. Electrochem. Soc.* **1957**, *104* (3), 182–194.